Bulletin of the Seismological Society of America, Vol. 75, No. 4, pp. 1021–1040, August 1985

APPLICATION OF WAVEFORM MODELING TO DETERMINE FOCAL MECHANISMS OF FOUR 1982 MIRAMICHI AFTERSHOCKS

BY CHANDAN K. SAIKIA AND ROBERT B. HERRMANN

ABSTRACT

The objective of this study is to determine the focal mechanisms of small earthquakes at very near epicentral distances and use them to predict the observed waveforms. To achieve our objectives, the following steps were adopted before attempting to match the entire waveform: (a) obtain an appropriate velocity model; (b) calculate the Green's functions and predict ground motions due to an earthquake specified by dip (δ), slip (λ), and strike (φ) of a fault; (c) select all mechanisms which satisfy the first-motion polarity at all stations; (d) select a subset of focal mechanisms from those obtained in step (c) which produce *P* and *S* amplitudes and *P/SV* and *SV/SH* amplitude ratios correctly; and (e) use focal mechanisms of step (d) to match waveforms. As an alternative approach, a least-squares inversion for the moment-tensor elements was performed and decomposition of moment tensor matrix to two double couples (major and minor) was performed. Green's functions were computed using the Cagniard-de-Hoop theory (Helmberger and Harkrider, 1978).

We applied the above approaches to four aftershocks ($m_{bLg} \leqq 3.5$) of the New Brunswick earthquake of 9 January 1982 and succeeded in obtaining focal mechanisms and producing synthetic waveforms very similar to the observed waveforms. Two groups of focal mechanisms are found. Two of the earthquakes are found to have reverse fault geometry similar to that of the main event of 9 January 1982 (m_b = 5.7), while the other two have significant components of strike-slip motion on a dipping plane. The results obtained from the least-squares analysis support the results of the search method. The fault geometries determined by the search method correspond well to the results of the major double couple of the least-square inversion.

For completeness of the source characteristics investigation, spectral analysis of the seismograms was performed to determine the source parameters: corner frequencies, f_c, seismic moments, source dimensions, and stress drops.

INTRODUCTION

Studies of small earthquakes recorded digitally at short distances are drawing attention from seismologists because they provide information about the physics of the earthquake source process without too much contamination due to wave propagation. Focal mechanisms can be determined for individual event or for composites of events using the first-motion information of direct P waves. Some seismologists (Kisslinger, 1980; Snoke *et al.*, 1984) have used the $(SV/P)_z$ amplitude ratios from vertical component seismograms, together with P-wave first-motion polarities, to determine the focal mechanisms of individual earthquakes. Inclusion of the amplitude ratio data helps make up for an imperfect sampling of the P-wave first-motion data on the focal sphere as well as for a lack of horizontal component seismograms. These amplitude ratio methods are based on the assumption that the transmission coefficients at the structural interfaces have small influence on the amplitude ratios. An implicit assumption is that the phases used are in fact the direct P- and S-wave arrivals. Another fundamental assumption is that the earth can be reasonably approximated as a half-space in order to correctly match observed amplitude ratios at the free surface. In many cases, this assumption is invalid, as evidenced by the

difference between the amplitude partition of P and SV arrivals on the vertical and radial components. A proper account of earth structure is required.

A powerful way to do this is to construct synthetic seismograms for a realistic earth model and arbitrary fault geometry and then to compare these synthetics to observed data. A systematic synthesis and comparison between observed and predicted waveforms is possible but time consuming.

The object of this paper is to develop a realistic approach to the problem of using waveform matching to determine the focal mechanisms of earthquakes recorded at short distances. Cagniard-de Hoop techniques will be used for the generation of ground motion synthetic seismograms. This study will be confined to the direct P- and S-wave arrivals. However, it is possible to use both the body- and surface-wave information present in such data (Burdick *et al.*, 1984). The approach used in the present paper was developed during the analysis of some digitally recorded aftershocks of the Miramichi earthquake of 9 January 1982 (Cranswick *et al.*, 1982).

Modeling and Search Techniques

The theory of Cagniard-de Hoop synthesis technique has been published in a number of papers (Helmberger and Harkrider, 1978; Heaton, 1978). Following Helmberger and Harkrider (1978), the ground displacements due to step dislocation in a cylindrical coordinate system are as follows

$$
\begin{aligned}
w(t, r, z, \vartheta) &= \frac{M_0}{4\pi\rho_0}\frac{d}{dt}\left[\dot{S}(t)^* \sum_{j=1}^{3} H_{w_j}(t, r, z)A_j(\vartheta, \lambda, \delta)\right] \\
q(t, r, z, \vartheta) &= \frac{M_0}{4\pi\rho_0}\frac{d}{dt}\left[\dot{S}(t)^* \sum_{j=1}^{3} H_{q_j}(t, r, z)A_j(\vartheta, \lambda, \delta)\right] \\
v(t, r, z, \vartheta) &= \frac{M_0}{4\pi\rho_0}\frac{d}{dt}\left[\dot{S}(t)^* \sum_{j=4}^{5} H_{v_j}(t, r, z)A_j(\vartheta, \lambda, \delta)\right] \qquad (1)
\end{aligned}
$$

where w, q, and v are the vertical, radial, and transverse displacements, respectively, and for details, see Helmberger and Harkrider (1978). We define A_j's in terms of the vector $\boldsymbol{n}(n_1, n_2, n_3)$ normal to the fault and the direction of slip $\boldsymbol{f}(f_1, f_3, f_3)$ as

$$
\begin{aligned}
A_1 &= (f_1n_1 - f_2n_2)\cos 2(AZ) + (f_1n_2 + f_2n_1)\sin 2(AZ) \\
A_2 &= (f_1n_3 + f_3n_1)\cos(AZ) + (f_2n_3 + f_3n_2)\sin(AZ) \\
A_3 &= f_3n_3 \\
A_4 &= (f_1n_1 - f_2n_2)\sin(AZ) - (f_1n_2 + f_2n_1)\cos 2(AZ) \\
A_5 &= (f_1n_3 + f_3n_1)\sin(AZ) - (f_2n_3 + f_3n_2)\cos(AZ) \qquad (2)
\end{aligned}
$$

where AZ is the azimuth of the station measured from the north and the n_i and f_i's are expressed in terms of δ, λ, and φ as

$$
\begin{aligned}
n_1 &= -\sin\delta\sin\varphi & f_1 &= \cos\lambda\cos\varphi + \sin\lambda\cos\delta\sin\varphi \\
n_2 &= \sin\delta\cos\varphi & f_2 &= \cos\lambda\sin\varphi - \sin\lambda\cos\delta\cos\varphi \\
n_3 &= -\cos\delta & f_3 &= -\sin\lambda\sin\delta. \qquad (3)
\end{aligned}
$$

To synthesize the ground motion, the numerical values of the A_j's, calculated using (2) and (3) for a particular combination of δ, λ, and φ, are used to combine Green's functions according to the expressions of equation (1). As can be seen from (1) to (3), the ground motion is a nonlinear function of the fault parameters. The expressions A_j can be expressed in terms of the moment-tensor elements (M_{ij}) (Mendiguren, 1977) of a deviatoric point source as given by Langston (1981)

$$A_1 = \frac{1}{2}(M_{22} - M_{11})\cos 2(AZ) - M_{12}\sin(AZ)$$

$$A_2 = -M_{13}\cos(AZ) - M_{23}\sin(AZ)$$

$$A_3 = \frac{1}{2}(M_{11} + M_{22})$$

$$A_4 = -\frac{1}{2}(M_{11} - M_{22})\sin 2(AZ) + M_{12}\cos 2(AZ)$$

$$A_5 = -M_{23}\cos(AZ) + M_{13}\sin(AZ). \tag{4}$$

When these expressions are substituted in (1), the expressions for the ground motion become linear with respect to the M_{ij}'s provided the source-time function is known. For small nearby earthquakes with high corner frequencies, the direct waves can be treated as the impulse responses of the medium and so the source-time functions can be assumed known. This is especially true if the recorded data are low-pass filtered. As will be seen later, this assumption has led to a very simple least-squares formulation for the moment-tensor elements, which will also be used to complement the search procedure.

There are a number of factors that influence the waveforms. In particular, producing the correct Green's functions involves lot of trials on the earth model. If the entire waveform match is sought immediately, it will take enormous computation effort to simultaneously determine source parameters and earth model. Therefore, it is necessary to start with specified phases to isolate all possible focal mechanisms before attempting a waveform inversion. Since the digital data were obtained at short distances, the waveforms are relatively simple. The *P*- and *S*-wave arrivals are usually distinct phases. Thus, the inversion procedure makes the maximum use of the pulse amplitudes rather than the entire waveform of each arrival. In order to predict these focal mechanisms and then the waveforms, we proceed as follows

(a) Determine a viable velocity model: Besides defining gross crustal structure, it is very necessary to define the shallow structure near the receiver. The model must be able to predict the observed partition of *P*-wave amplitude on the vertical and radial components and also the observed partition of *S*-wave amplitude on the vertical and radial components. This in turn requires that the *P*- and *S*-wave arrivals be distinct. The partition of amplitude at the free surface is a function of the surface velocities. This is, in fact, a difficult task if no *a priori* information about the earth model is available and will require many trials. The earthquake hypocenter is then located using this new earth model.

(b) Calculate the Green's functions: Using the earth model, compute the Green's functions of equation (1). Convolve the Green's functions with the appropriate instrument response and source-time function.

(c) Search 1: Search through all possible focal mechanisms, saving only those focal mechanisms which satisfy P-wave first-motion data. The objective function is defined as the vector dot product between two multi-dimensional unit vectors, one consisting of observed P-wave first-motion polarities and the other of the predicted P-wave first-motion polarities. This is equivalent to obtaining a correlation coefficient between the two data sets, with the constraint that the means of each data set be identically zero.

(d) Search 2: Find the subset of focal mechanisms passed in step (c) which satisfy P/SV and SV/SH amplitude ratios correctly. This is quickly done by forming a table of observed amplitude ratios and by forming a list of the Green's function amplitudes of the P- and S-wave arrivals, and then quickly computing theoretical amplitudes for each focal mechanism. As a goodness-of-fit criterion, the unit vector dot products between observed and predicted P- and S-wave amplitudes and between observed and predicted amplitude ratios must both be maximized. Specifying minimum values of the vector dot products yields a suite of possible focal mechanisms.

(e) Test 1: Using the focal mechanisms satisfying step (d), determine the subset that satisfies observed P- and S-wave amplitudes on all components at all stations. This step involves the determination of the seismic moment, which is estimated using the observed and predicted amplitude vectors. If there is some disagreement, vary the focal depth and return to step (b).

(f) Test 2: Test each mechanism of step (d) in the neighborhood of the best focal parameters for the best waveform fit. At this point, synthetic waveforms are generated. If the waveforms do not agree with the observed waveforms, the earth model should be modified and every step should be repeated.

(g) Moment-tensor inversion: The convergence of the systematic search techniques of steps (c) to (f) guarantees that the earth model and focal depth are reasonably well known. Perform a moment-tensor inversion using the observed P- and S-wave amplitudes on all components and the corresponding amplitudes on the Green's functions.

To facilitate comparison of actual data and synthetics based on simplified earth models, both the observed data and the theoretical Green's functions are passed through an identical low-pass filter. In doing this, it was hoped that the need for very detailed earth structure would be minimized.

The Miramichi Data Set

Following the earthquake of 9 January 1982 (46.90°N, 66.66°W, NEIS; $m_b = 5.7$) in the Miramichi region of New Brunswick, Canada, the U.S. Geological Survey employed a portable digital network consisting of both three-component velocity and acceleration meters from the 15 to 22 January 1982 with the cooperation of the Canadian Department of Energy, Mines and Resources, Ottowa. This network recorded about 40 aftershocks suitable for the spectral study. Preliminary locations of these events are published in the U.S. Geological Survey Open-File Report (Cranswick *et al.*, 1982). The aftershocks are small in magnitude, the largest one being of magnitude $m_{Lg} = 3.5$.

The focal mechanism of the main earthquake ($m_b = 5.7$) was determined from the teleseismic body-wave observations (Choy *et al.*, 1983) and also from continental surface-wave observations (Wetmiller *et al.*, 1984). Wetmiller *et al.* (1984) also

included the composite focal mechanisms of the aftershock sequence for the months of January and April through June using the observations at near distances.

For the present paper, we have applied the waveform match technique to four aftershocks of the area. Figure 1 shows the station positions and the free-depth locations of the aftershocks of this study. The instruments were located at four different locations: C7V; C8V; C9V; and CBA. Sites C7V and C8V were equipped with both force balance accelerometer and velocity sensors, whereas the site C9V was equipped with only a velocity sensor and the site CBA with only an accelerometer. The detailed information about these instruments can be obtained from Cranswick *et al.* (1982).

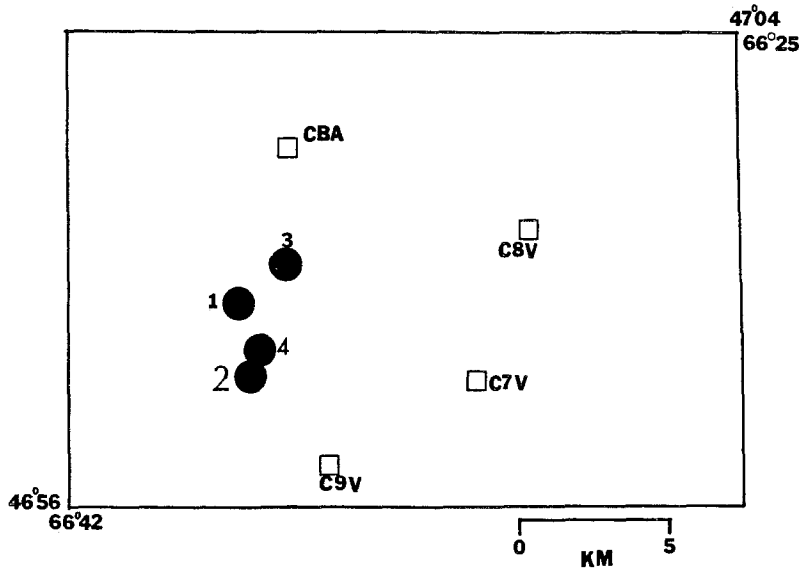

FIG. 1. Map showing station locations (squares) and relocated epicenters (solid circles). The coordinates corresponding to the numbered events are given in Table 1.

AFTERSHOCK LOCATION

Preliminary locations of all 40 aftershocks reported earlier by Cranswick *et al.* (1982) were determined using a homogeneous half-space velocity model (6.2 km/sec for P wave and 3.57 km/sec for S wave). But the nature of the signals present in the observed seismograms suggested that the source region is better represented by a layered medium, which was also confirmed by Cranswick (personal communication). According to Cranswick, the source region can be modeled by three layers overlain by a thin sedimentary cover of varying thickness, from a few meters to a few hundred meters. The most likely ratio of P- to S-wave velocity is 1.73. We had to modify this model in order to match free surface amplitude partition. Four aftershocks were located with respect to this modified velocity model using both P- and S-arrival times. The arrival time of the S phase was picked from the horizontal components. These times were entered into the location program FASTHYPO (Herrmann, 1979). The S-wave velocity in each layer was determined within the program, using the P- to S-wave velocity ratio as 1.73. Both free and fixed-depth options were used to locate the aftershocks. The criterion for the best location was

to obtain the minimum residuals between the observed and the calculated travel times. Sometimes, the depth of the earthquake was fixed beforehand to make the ray path conform to the free surface particle motion of the direct P wave. It may be noted that the epicenters do not change significantly even if the depths of the aftershocks are varied substantially. Table 1 shows both our and earlier (Cranswick *et al.*, 1982) locations of the aftershocks studied in the present paper. Table 2 presents the starting and final velocity models. The final velocity model is used to generate the required Green's functions.

TABLE 1

HYPOCENTRAL LOCATION OF THE AFTERSHOCKS (FREE DEPTH)

Event	Date	Origin Time (UTC)	Latitude (°N)	Longitude (°W)	Depth (km)	No. of Phases	No. of Stations
1	17 Jan. 1982	13:33:55.71	46.98	66.61	4.89 ± 0.21	6	3
	C*	13:33:56.2	46.99	66.63	3.61	6	3
2	17 Jan. 1982	13:32:59.89	46.99	66.63	2.40 ± 0.05	5	3
	C	13:32:59.9	46.99	66.63	2.60	6	3
3	18 Jan. 1982	19:34:49.17	47.01	66.61	3.51 ± 0.15	6	3
	C	19:34:49.2	47.00	66.61	5.31	6	2
4	21 Jan. 1982	00:39:55.72	46.98	66.60	4.77 ± 0.13	6	3
	C	00:39:55.7	46.98	66.61	4.85	6	3

* C, published by Cranswick *et al.* (1982), free depth (P velocity: 6.2 km/sec; S velocity: 3.57 km/sec).

TABLE 2

EARTH MODELS

P Velocity (km/sec)	S Velocity (km/sec)	Density (gm/cm^3)	Thickness (km)
Initial Model (Cranswick, personal communication)			
—	—	—	—
5.4	3.1	—	0.5
5.8	3.3	—	3.0
6.2	3.6	—	∞
Velocity Model of Present Study			
4.4	2.2	2.2	0.2
4.9	2.62	2.3	0.2
5.4	3.12	2.4	0.2
5.8	3.25	2.5	2.9
6.2	3.58	2.65	∞

DATA ANALYSIS

The observed data seem to have impulsive P- and S-wave arrivals with the P wave well developed generally on the vertical components and the S wave on the horizontal components. All events recorded at the site C7V have similar frequency content in all three components, but at site C8V the frequency content is conspicuously different between the traces. The vertical components contain higher fre-

quencies than does the horizontal components. In addition, the seismograms at site C8V are more complicated, perhaps due to site effects. Therefore, the observed seismograms were convolved with a third-order causal Butterworth filter (corner at 10 Hz) so that the direct P and S phases appear much like impulse responses of the Butterworth filter.

All Green's functions were calculated using only the far-field asymptotic terms since we were interested only in high-frequency signals. We used the computer program GENRAY81 written by Dr. Charles A. Langston for computing the Green's functions. To represent the wave field adequately, we calculated the medium response initially including many rays, particularly all converted rays at each interface. Because of the low-pass filter, the simple earth model, and the short source-receiver distances, the direct rays were found to be dominant contributors to the seismograms. The source-time function was approximated by using a symmetrical triangular-shaped pulse with a total duration of 0.04 sec. Seismograms were synthesized at a sampling interval of 0.01 sec. The source-time function used has a spectral hole at the Nyquist frequency, and hence will not generate spurious edge effects when using Fourier transform techniques. For the signals studied, this source pulse provides an effective impulse response of the medium. Its corner frequency is approximately 25 Hz. The instrument response (natural frequency 2.0 Hz and damping coefficient 0.6) is included in the synthetics by using a recursive digital filter. The Green's functions were identically filtered and were retained for later analysis. The effect of an elastic attenuation on the Green's functions was assumed negligible, since the average Q-factor for the New Brunswick area is about 1900 at a frequency of 10 Hz (Shin and Herrmann, in preparation).

Several tests were performed for the medium parameters. Cranswick's half-space model produced good fits to the shapes of the waveform, but failed to produce correct amplitude ratios. The similarity of shapes indicated that the filtered observed waveform data were entirely shaped by the Butterworth and instrumental filter effects, and that the source-time function is in fact of very short duration, as assumed. Next, the velocity model was changed to a layered model consisting of three layers with a Poisson's ratio of 0.25, also suggested by Cranswick. This velocity structure did not partition the incident P- and SV-wave amplitudes correctly at the free surface between the vertical and horizontal components. For example, the observed amplitude ratios of P_r/P_z and S_r/S_z of the aftershock of 17 January 1982 (13h33m55.71s) are approximately 0.716 and 2.23 for C7V and 1.19 and 1.867 for C8V, respectively. Theoretically for such amplitude ratios and for a velocity model with $\alpha = 1.73\beta$ (where α is the P-wave velocity and β is S-wave velocity), the direct P wave should be incident at the free surface at stations C7V and C8V at angles 32.0° and 33.5° and S wave at angles 47.0° and 36.5°, respectively. With respect to the depth and epicentral distances obtained from the Cranswick's initial model, Table 2, the direct rays for this aftershock do not have these angles. We varied the depth to obtain these angles, but this produced a strong surface refracted SP phase at station C8V which is not observed. To resolve this problem, we computed the normalized amplitudes for the radial and vertical components with respect to a unit incident wave for all possible angles of incidence from 0° to 90° for P- to S-velocity ratios equal to 1.73, 1.8, and 2.0 and found that a ratio of 2.0 is likely at the surface layer. The P velocity required a gradient form of decrease near the surface. The final velocity model selected for this study is as given in Table 2. This velocity model was tested for the amplitude ratios of other three earthquakes too. While it is difficult to obtain a single velocity model which can satisfy the amplitude ratios

of high-frequency signals of all earthquakes at all stations simultaneously and absolutely, the new velocity model can produce the observed amplitude ratios within a small trade-off. So the suggested velocity model can be treated as reasonable.

Results of Waveform Modeling

Using the hypocenter locations, the observed horizontal component data were rotated to form radial and tangential time histories. The lack of P-wave arrivals on the tangential component was taken as indication that the source-receiver azimuth was properly determined. As convention for both the synthetic and observed seismograms, positive amplitudes on the vertical, radial, and tangential components correspond to ground motion up, away from the source, and in a clockwise direction about the source when looking down at the source. The units for all trace amplitudes in the seismograms presented are centimeters/second.

(1) 17 January 1982 (origin time 13h33m55.71s). This aftershock was modeled using the velocity sensor data of two stations, C7V and C8V. The filtered seismograms at site C7V (Figure 3, left) were in fact simple. In comparison, the seismograms at site C8V (Figure 3, right) are much more complicated probably due to the trapped energy within the sedimentary layer. The S phase in the radial component of site C8V is broad due to the likely interference from other phases. We rule out the source-time function as a possible factor because the vertical and tangential components at C8V and all components at site C7V have similar durations for both P and S pulses.

The Green's functions were computed at various depths using the modified earth model of Table 2 to search for the focal mechanisms. Those calculated at a depth of 6.0 km fit the observed data best. Each time the depth was varied, the aftershock was relocated and, as expected, the residuals in travel times changed. Moreover, there was an apparent time difference for the S-P travel time between the programs GENRAY81 and FASTHYPO, because FASTHYPO assumed $\alpha = 1.73\beta$ in each layer which GENRAY81 used α and β values as defined in the model. To compensate for this, the epicentral distances were adjusted for S-P times using a simple ray theory formulation. The final epicentral distances for stations C7V and C8V were 5.0 and 8.1 km, respectively, and source-receiver azimuths were 95° and 70°, respectively. Following the outlined procedure, all possible focal mechanisms which had positive unit vector dot products for the P- and S-wave polarities and their amplitude ratios were obtained. For this aftershock, the unit vector dot product for the P-wave amplitude was generally poor. So we have selected all the solutions having a unit vector dot product greater than 0.7 for S amplitudes and 0.9 for the amplitude ratios. All these possible focal mechanism solutions are plotted in Figure 2a. Next the amplitude constraint was applied to obtain the best mechanism which had the following parameters: dip = 42.0°; slip = 175.0°; and strike = 43.0°. This mechanism suggests that the aftershock is caused by thrust faulting with a significant portion of strike-slip motion, and the associated fault dips towards the southeast. Although this mechanism does not correspond to any of the composite focal mechanisms of Wetmiller *et al.* (1984, Figure 14), we still believe that our mechanism is valid, as the results from the least-squares inversion are also identical. Further, unless the source area is quite localized in space, the composite focal mechanism will not necessarily represent the true rupture at the faulting zone for all earthquakes.

As an alternative approach to the search technique, we also inverted for the moment-tensor elements. A standard least-squares procedure (Wiggins, 1972) is used to invert for the moment tensor elements. To perform the generalized inversion, the programs of Lawson and Hanson (1974) were adopted. Similar to the search technique, we carried the least-squares inversion for the moment-tensor elements using the amplitude and polarity information of *P*, *SV*, and *SH* waves. The eigenvalues were calculated. For a pure double-couple mechanism, the intermediate stress must be zero and, since it was not so, the moment tensor matrix was decomposed to a pair of orthogonal double couples: major and minor. The parameters of the double-couple mechanisms and the moment-tensor elements are given in Table 3. The per cent of the compensated linear vector dipole (CLVD) is 25.01. The lower hemisphere projection of the decomposed major double-couple is shown

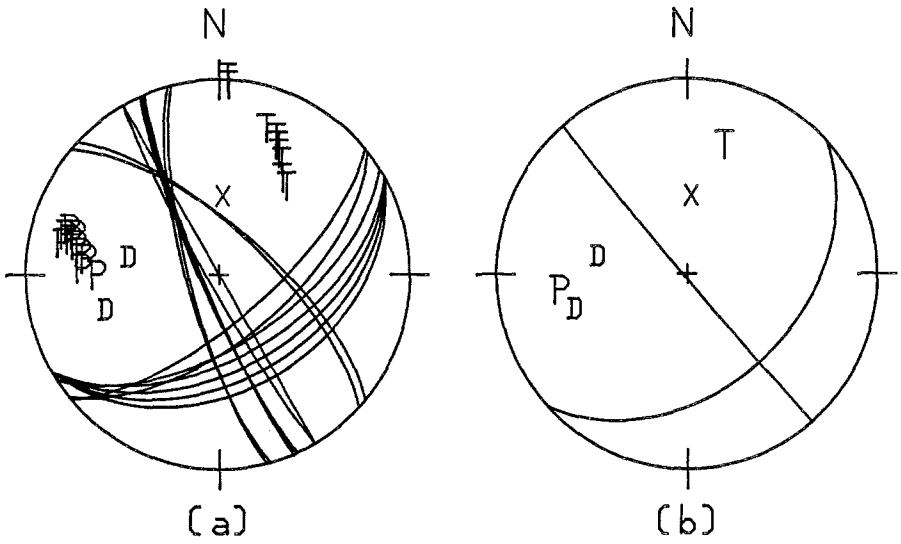

FIG. 2. Focal mechanisms of event 1. (a) Admissible solutions using search technique with data from stations C7V and C8V. (b) Major double-couple solution using moment-tensor inversion. In this and other focal mechanism plots to follow, the symbols D and C represent observed dilatational and compressional *P*-wave first motions, respectively, and the symbols *P* and *T* represent the locations of the pressure and tensions axes, respectively, for a particular set of nodal planes. Lower hemisphere, equal-area projections are used.

in Figure 2b. The *T* axis of this mechanism trends toward the northeast (azimuth = 11.41° and plunge = 34.74°) and the *P* axis toward the southwest (azimuth = 257.91° and plunge = 29.89°) directions. The scalar seismic moment estimated from the moment-tensor matrix by dividing the modulus of the moment tensor by $\sqrt{2}$ is $4.088e{+}20$ dyne-cm.

The synthetic seismograms for this aftershock are shown in Figure 3 for stations C7V and C8V. The radial component of the station C8V is not well modeled since the synthetic seismograms did not contain many reverberations within the layers. We considered only 12 rays which included three direct body-wave phases (*P*, *SV*, and *SH*). Since the impedance contrast at the interface is not very large, the converted rays did not have enough energy to show up in the synthetics. All the synthetic seismograms are predicted using the seismic moment $3.29e{+}20$ dyne-cm obtained by averaging the values calculated for each component. The amplitudes are within a factor of 2 of the corresponding observed amplitudes.

(2) 17 January 1982 (origin time 13h32m59.89s). This aftershock is also modeled using the data of the two stations C7V and C8V. The Green's functions computed at a depth of 5.5 km fitted the observed data best. The epicentral distances for the stations C7V and C8V were adjusted as before at 5.3 and 7.2 km, respectively. The wave shapes of this aftershock are similar to those of aftershock of 17 January 1982 (13h33m55.71s). Therefore, as expected, the focal mechanisms of these two aftershocks were found to be nearly the same. The search technique produced many solutions (Figure 4a) whose synthetic seismograms had good wave shape match but poor amplitudes ratios. For good agreement in amplitudes, the azimuths of the stations as well as the focal parameters of the solutions of search technique were

TABLE 3

SUMMARY OF RESULTS

	17 January (13:32:59.89)	17 January (13:33:55.71)	18 January (19:34:49.17)	21 January (00:39:55.72)
Inversion results (dyne-cm):				
M_{xx}	−0.193*e*+20	−2.450*e*+20	−0.573*e*+20	−0.698*e*+19
M_{yy}	0.225*e*+20	2.478*e*+20	0.175*e*+20	0.239*e*+20
M_{xy}	0.411*e*+18	−0.299*e*+20	0.207*e*+20	0.149*e*+20
M_{yz}	−0.241*e*+20	−1.599*e*+20	−0.563*e*+20	−0.102*e*+20
M_{zx}	−7.014*e*+20	−2.827*e*+20	0.650*e*+20	0.905*e*+19
Moment (M_0)	0.330*e*+20	4.088*e*+20	1.783*e*+20	0.296*e*+20
Double-couple				
Major				
Dip (δ)	40.7	40.9	63.4	63.5
Slip (λ)	177.5	175.5	121.6	134.6
Strike (φ)	47.3	42.3	205.1	190.3
Minor				
Dip (δ)	86.7	24.8	17.0	9.5
Slip (λ)	64.9	−16.4	−53.5	−35.6
Strike (φ)	253.3	157.5	78.7	124.0
% of CLVD	32.81	25.01	11.6	9.4
Search results:				
Dip (δ)	41.0	42.0	63.0	60.0
Slip (λ)	177.0	175.0	121.0	130.0
Strike (φ)	47.0	43.0	205.0	190.0
Moment (M_0) (dyne-cm)	0.245*e*+20	3.290*e*+20	1.450*e*+20	0.268*e*+20
Depth in km	5.5	6.0	7.0	6.0

varied within about ±10°. This process produced a solution with the parameters: dip = 41°; slip = 177°; and strike = 47° as the best possible candidate. The azimuth of C7V was adjusted at 102° and of C8V at 65°.

The moment tensor elements, Table 3, obtained from the least-squares inversion had identical parameters in terms of dip, slip, and strike for the major double-couple mechanism (Figure 4b, lower hemisphere projection). The T axis trends toward the northeast (azimuth = 15.48° and plunge = 33.75°) and the P axis toward the southwest (azimuth = 261.72° and plunge = 31.07°) directions. The per cent of CLVD is 32.81. The scalar seismic moment is estimated from the moment-tensor elements and is 3.30*e*+19 dyne-cm.

The synthetic seismograms computed for the two stations at C7V and C8V with seismic moment of 2.45*e*+19 dyne-cm are shown in Figure 5. In general, the

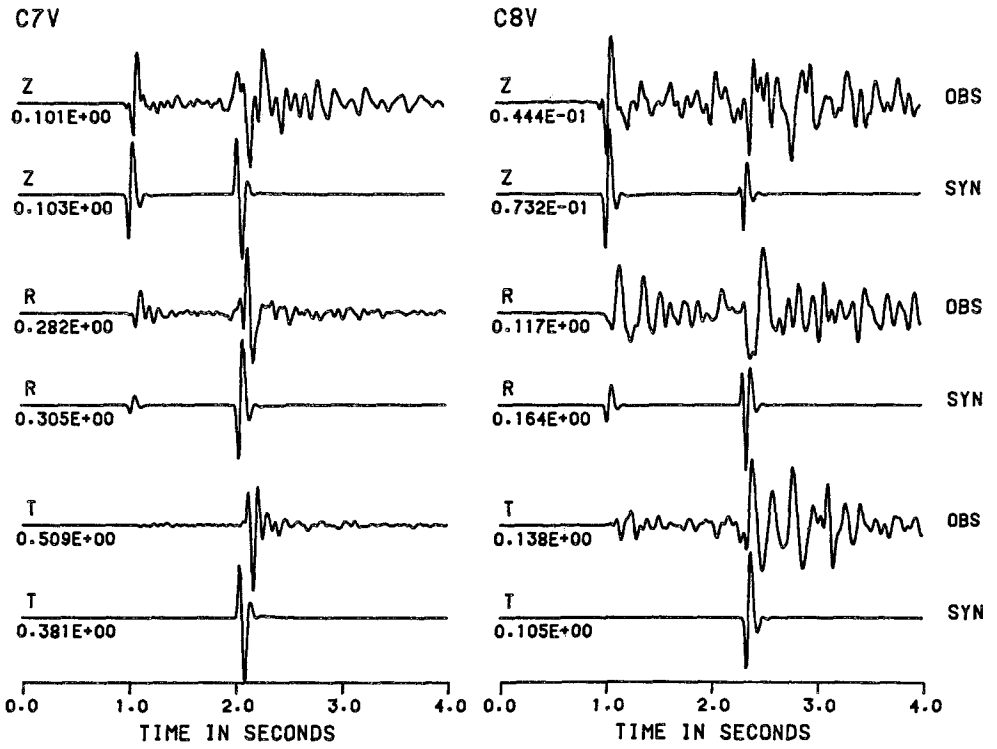

FIG. 3. Comparison of observed and predicted filtered seismograms at stations C7V and C8V for event 1. Trace units are in centimeters/second of ground motion.

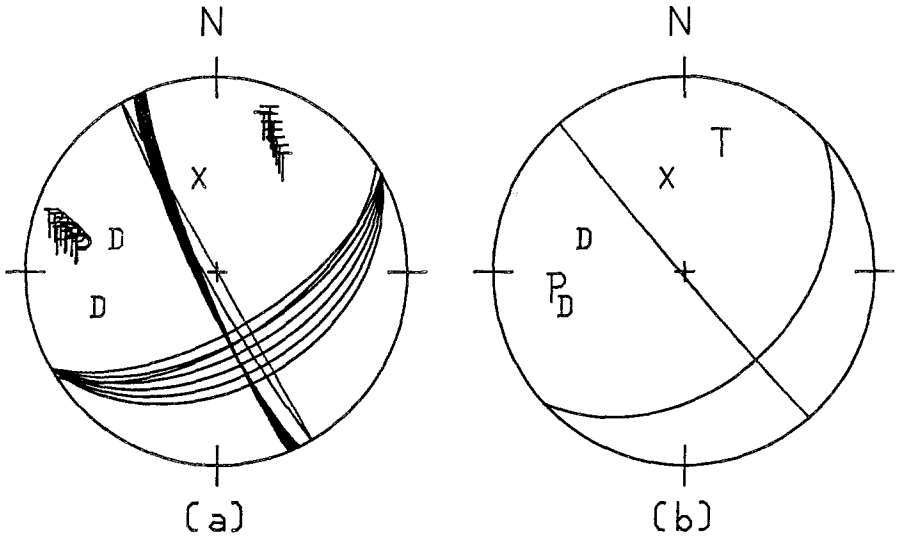

FIG. 4. Focal mechanisms for event 2. (a) Admissible solutions using the search technique with data from stations C7V and C8V. (b) Major double-couple solution using moment-tensor inversion.

agreement of the wave shapes and the amplitude ratios between synthetic seismograms and observed seismograms is very good.

(3) 18 January 1982 (19h34m49.17s). This aftershock is modeled using the data of the stations C9V and C8V. Green's functions were computed at an epicentral

distance of 4.3 km for station C9V and 6.0 km for station C8V at a depth of 7 km. The search technique produced many possible solutions. We retained only those solutions which also satisfied the polarity at station C7V (vertical component). In Figure 6*a*, we plotted the solutions having unit vector dot products for P and S waves greater than 0.92 and for the amplitude ratios greater than 0.9. The best solution which finally produced the correct amplitude ratios has the following focal parameters: dip = 63°; slip = 121°; and strike = 205°. The azimuth of C9V was adjusted at 182° and C8V at 87°.

The least-squares inversion for the moment-tensor elements, Table 3, and decomposition to the major and minor double couples were performed. Figure 6b shows the solution obtained for the major double couple. The T axis trends toward the

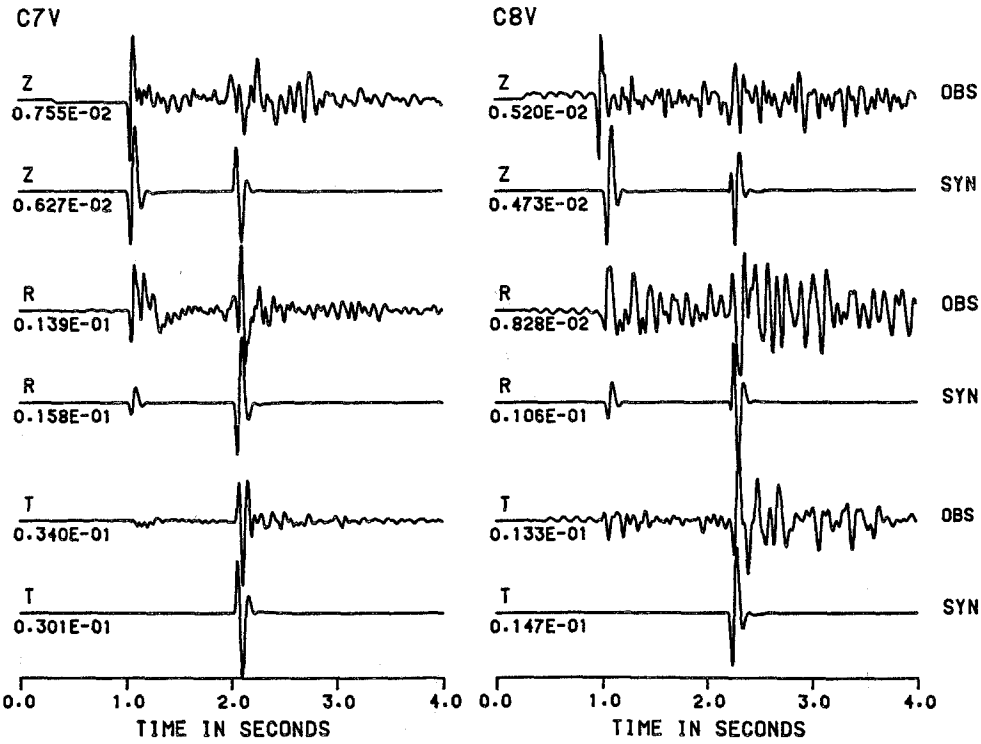

FIG. 5. Comparison of observed and predicted seismograms at stations C7V and C8V for event 2.

southeast (azimuth = 160° and plunge = 58.77°) and the P axis toward the southwest (azimuth = 267.14° and plunge = 12.87°) directions. The CLVD is 11.6 per cent. The scalar seismic moment from the moment-tensor matrix is 1.783e+20 dyne-cm.

Figure 7 shows the synthetic seismograms at stations C7V and C9V, respectively, computed using the focal mechanism obtained from the search technique. An average seismic moment of 1.45e+20 dyne-cm was used to predict the synthetic seismograms. The S-P travel-time interval in the synthetics is in agreement with the observed S-P travel-time interval. Whatever mismatch of phases seen in the seismograms can be adjusted by shifting either the observed or the synthetic trace, as the starting time in either is quite arbitrary. The S phase in the vertical component at C9V in the observed data appears complicated, and we could not model it perfectly since the high-frequency signals arriving immediately following the direct wave could not be predicted. Because of this, the amplitudes of the S

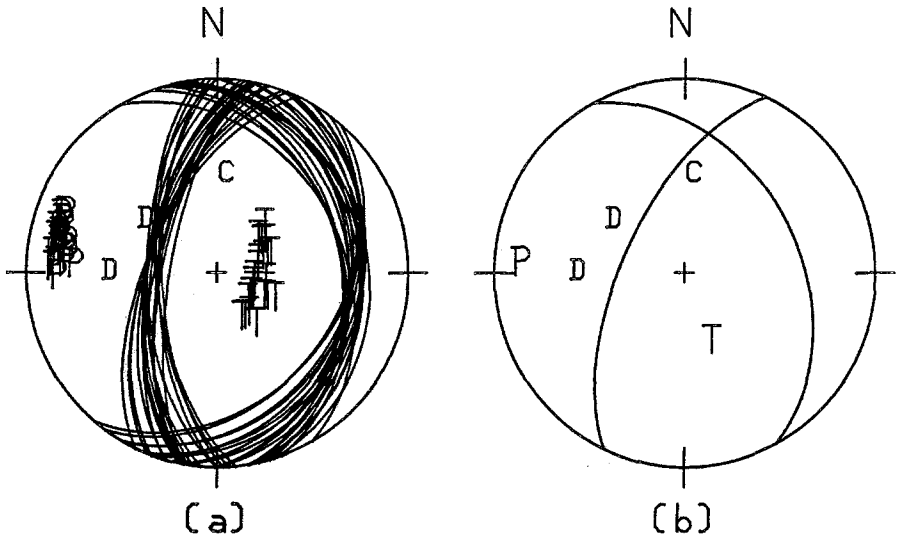

FIG. 6. Focal mechanisms for event (3). (a) Admissible solutions using search technique with data from stations C8V and C9V. (b) Major double-couple solution using moment-tensor inversion.

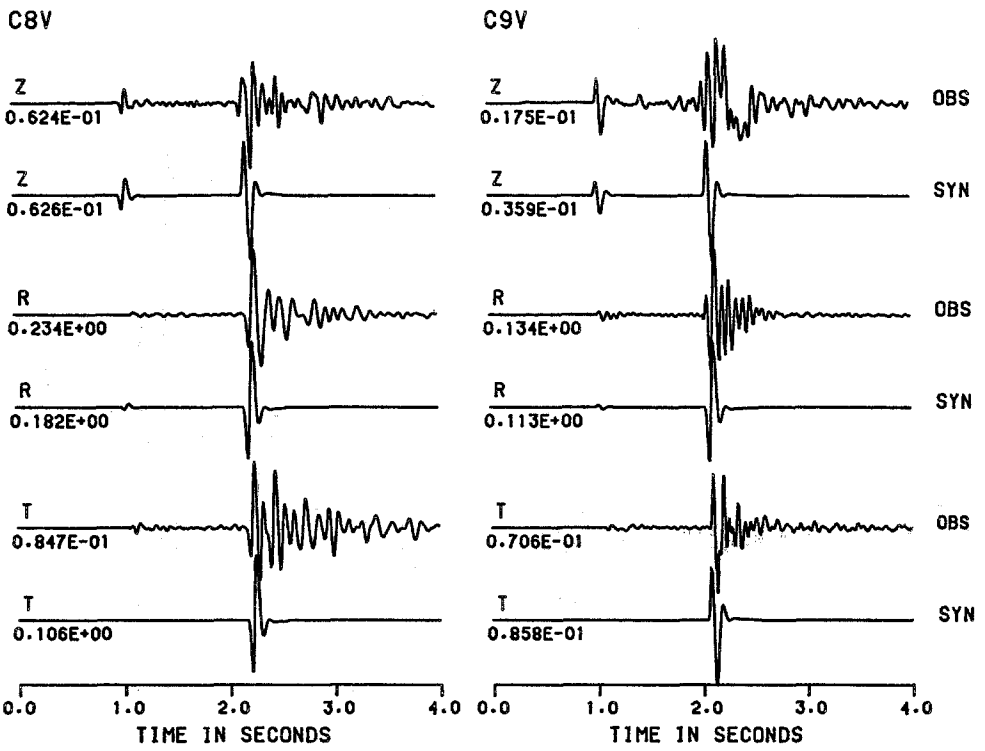

FIG. 7. Comparison of observed and predicted filtered seismograms at stations C8V and C9V for event 3.

phase in this component of C9V must have been affected. The seismic moment used for this aftershock may also partly cause this amplitude difference. Otherwise, the amplitudes of the predicted phases are in agreement with the observed phases and are within permissible error.

(4) 21 January 1982 (*00h39m55.72s*). This aftershock is modeled using the data of two stations, C9V and C8V. Station C7V recorded only the vertical and the EW components. Therefore, we decided to predict all the focal mechanisms using the amplitude information from only stations C8V and C9V. The *P*-wave first-motion data at C7V is used as a constraint. The search results are similar to the mechanism of the main earthquake of 9 January 1982 as obtained by Wetmiller *et al.* (1984). The Green's functions were computed at distances of 1.6 and 7.1 km for stations C9V and C8V, respectively, at a depth of 6 km. Figure 8a shows all the possible focal mechanisms with unit vector dot product greater than 0.85 for *P*- and *S*-wave amplitudes (polarities included) and 0.7 for the amplitude ratios. The best amplitude agreement was obtained by a mechanism with the following parameters: dip = 60°; slip = 130°; and strike = 190°. The azimuth of C9V was adjusted at 201° and of C8V at 50°.

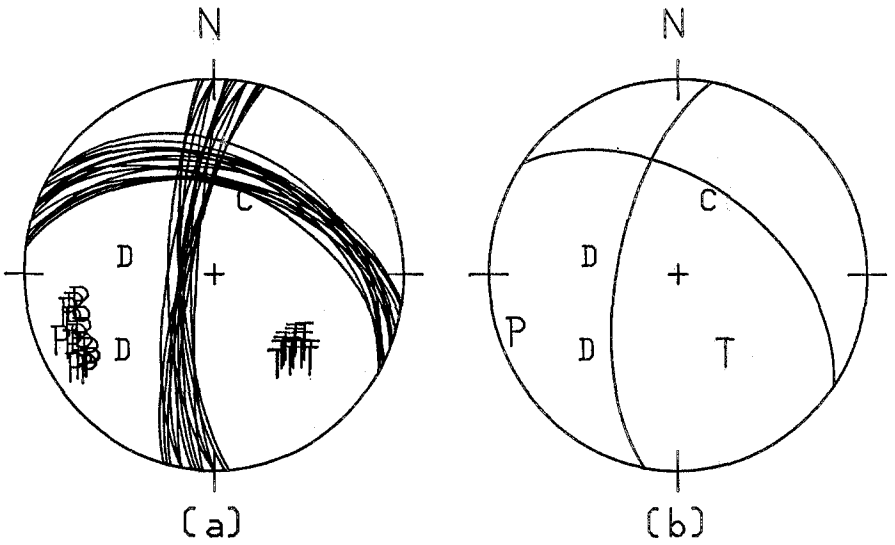

FIG. 8. Focal mechanisms for event 4. (a) Admissible solutions using search technique with data from stations C8V and C9V. (b) Major double-couple solution using moment-tensor inversion.

The double-couple focal mechanism obtained from the least-squares inversion is shown in Figure 8b and is similar to one obtained by the search technique. The *T* axis trends toward the southeast (azimuth = 150.82° and plunge = 49.96°) and the *P*-axis toward the southwest (azimuth = 250.16° and plunge = 7.76°). The scalar seismic moment estimated from the moment-tensor inversion is 0.296*e*+20 dyne-cm.

Figure 9 shows the synthetic seismograms predicted for stations C8V and C9V as well as C7V. The focal parameters are: dip = 63°; slip = 131°; and strike = 190° with seismic moment of 0.268*e*+20 dyne-cm. The relative wave shapes and the amplitudes of the synthetic seismograms match the observed seismograms well. The vertical synthetic *S* phase at station C8V has a very sharp upswing which is not observed in the real data. Even though the amplitude data at C7V were not used in the inversion procedure at all, the data fit at this station is quite good. This adds confidence to the focal mechanism obtained.

Spectral Analysis of the Aftershocks

Next spectral analysis was performed on the seismograms of these aftershocks to obtain the corner frequencies and the low-frequency spectral levels. The corner frequencies are related to the source dimensions and mean stress drops (Brune, 1970, 1971; Savage, 1972). Since aftershocks are recorded at very close stations (thus anelastic attenuation is negligible), the spectra of these microearthquakes may give us some information directly about the source. A representative pair of

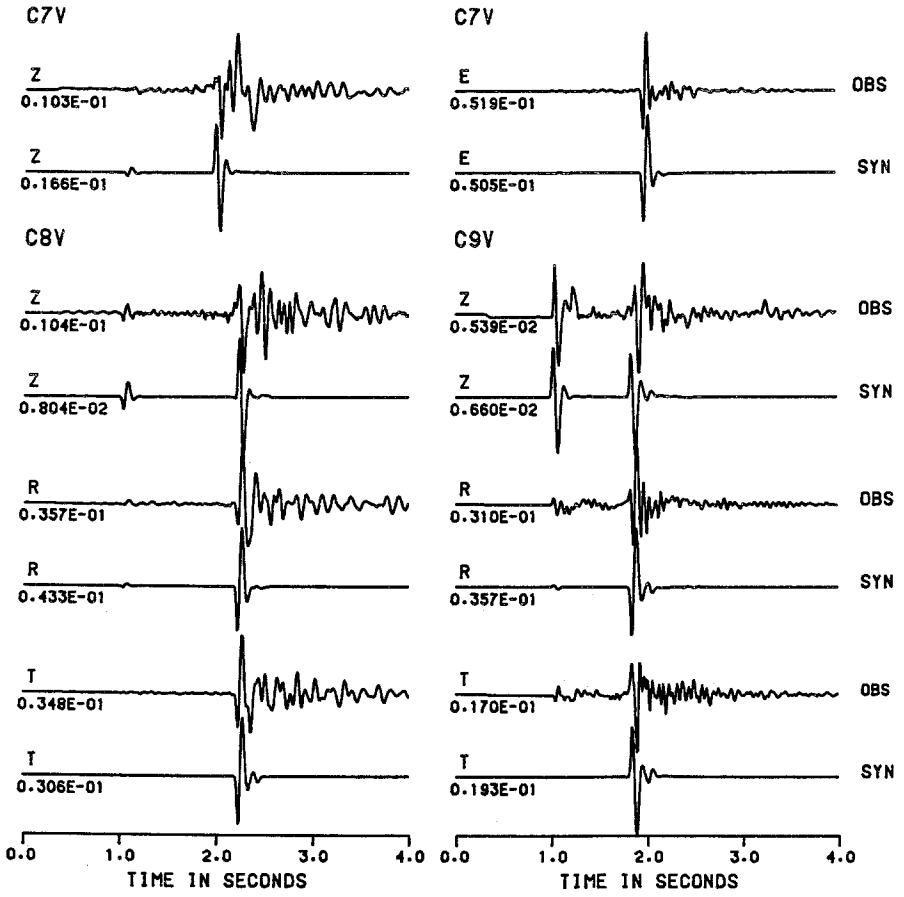

FIG. 9. Comparison of observed and predicted filtered seismograms at stations C8V, C9V, and C7V for event 4. The amplitude data at C7V were not used in the inversion, however the fit to the data is good.

spectral observations is given in Figure 10. The symbol to the upper right-hand corner identifies the aftershock and the component used for analysis. Arrows indicate the selected values for the low-frequency asymptotic and the corner frequency. Boatwright's (1972) expression was used in estimating the seismic moment. The radiation pattern was corrected using the expressions of Aki and Richards (1980, p. 115).

The digital seismograms were corrected for the gain of the instrument and possible DC offset. The *P*-wave spectra were computed from the windowed time-domain traces on the vertical components, and the *SV*-wave and *SH*-wave spectra were

computed from the windowed time-domain traces on the radial and tangential components, respectively, using fast-Fourier transformation. A 5 per cent cosine taper was used for windowing the signals. The window lengths of the time-domain seismograms were kept the same in all traces. The S wave was windowed such that, as pointed out by Archuleta and Hartzell (1981), the length of the signal incorporates the entire displacement pulse, including a few cycles of reverberating body-wave phases. The plots of log $A(\omega)$ versus log ω indicate fast decay of the amplitude level at high frequencies. The spectra were flat below the corner frequency which marked the long-period level. The slope of the high-frequency asymptote varied quite significantly. The long-period spectral levels, corner frequencies, spectral seismic moments, high-frequency slopes, source dimensions, and stress drops of the after-

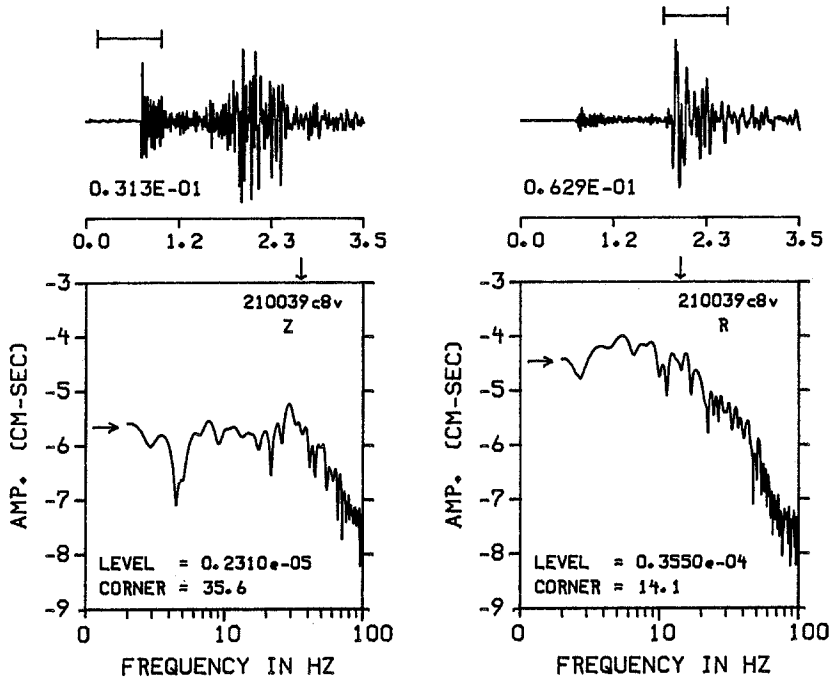

FIG. 10. Example of processed spectra data. The vertical and radial traces at station C8V are shown for event 4. A 0.80-sec time window is used to generate the spectra. The chosen low-frequency asymptote and corner frequency are indicated by arrows. The instrument-corrected displacement spectra are plotted on a log–log scale.

shocks are as given in Table 4. The source dimensions and stress drops were calculated using Brune's formula. The spectral levels, Ω_0, are given without any corrections due to the free surface and radiation pattern. The P-wave corner frequency is usually greater than the S-wave corner frequency for these aftershocks.

A comparison of the spectral modeling results given in Table 4 to the pulse-matching results given in Table 3 shows that there is excellent agreement for the 13:32 17 January 1982 event and the 19:34 18 January 1982 event. The spectral seismic moment for the 00:39 21 January event is four to six times larger than the waveform estimate, while the waveform seismic moment estimate exceeds the spectral estimate for the 13:33 17 January event by a factor of 2. We prefer the seismic moment estimated using the waveform modeling technique over the spectral technique since the dynamics of each ray are modeled.

TABLE 4

SOURCE PARAMETERS OF THE AFTERSHOCKS FROM SPECTRA

Event Station	Component	Ω_0 (cm-sec)	f_c (Hz)	M_0 (dyne-cm)	γ	r_s (km)	$\Delta\sigma$ (bars)	M_0 (log-av)	M_0 (lin-av)
0171332									
C7V	Z	0.111e−04	45.3	0.41	10.4	0.051	135.0		
	R	0.185e−04	27.1	0.25	5.4	0.049	90.1		
	T	0.389e−04	24.2	0.30	3.8	0.055	78.4		
C8V	Z	0.100e−04	30.0	0.48	6.1	0.071	45.9		
	R	0.152e−04	17.5	0.19	3.4	0.076	19.6		
	R	0.188e−04	17.5	0.23	3.1	0.076	22.4		
								0.29	0.31
0171333									
C7V	Z	0.351e−04	41.0	1.32	6.4	0.056	321.9		
	R	0.389e−03	17.9	3.84	4.6	0.075	406.5		
	T	0.731e−03	13.1	6.17	3.3	0.102	255.9		
C8V	Z	0.100e−04	36.9	0.41	5.7	0.063	71.9		
	R	0.512e−04	16.2	1.31	2.6	0.082	102.7		
	T	0.901e−04	18.3	2.32	4.3	0.073	261.7		
								1.84	2.56
0181934									
C8V	Z	0.162e−04	24.9	1.03	4.6	0.093	56.2		
	R	0.433e−03	11.0	2.81	3.9	0.121	68.8		
	T	0.100e−03	15.6	1.55	4.4	0.086	108.6		
C9V	Z	0.811e−05	50.0	1.40	5.7	0.046	622.3		
	R	0.165e−03	20.5	1.88	4.4	0.065	298.3		
	T	0.100e−03	23.6	1.09	4.1	0.055	263.8		
								1.53	1.63
0210039									
C8V	Z	0.231e−05	35.6	2.84	2.7	0.065	456.2		
	R	0.355e−04	14.1	0.63	2.8	0.095	32.8		
	T	0.433e−04	16.7	2.25	3.6	0.079	193.4		
C9V	Z	0.533e−05	45.3	0.44	3.6	0.051	146.3		
	R	0.481e−04	20.0	0.32	2.9	0.067	47.8		
	T	0.231e−04	22.0	1.97	2.5	0.061	240.5		
C7V	E	0.912e−04	27.0	2.73	6.3	0.049	989.8		
								1.17	1.60

The symbols used are: Ω_0, low-frequency spectral level before any correction (cm/sec); f_c, corner frequency (Hz); M_0, seismic moment from spectral study (dyne-cm $\times 10^{20}$); γ, high-frequency slope of displacement spectra; r_s, source dimension (km); $\Delta\sigma$, stress drop (bars); log-av, logarithmic average of seismic moment estimates; and lin-av, linear average of seismic moment estimates.

DISCUSSION AND CONCLUSIONS

In this paper, we have presented an approach by which the waveforms of high-frequency signals generated by small earthquakes at very short epicentral distances may be matched by determining the focal mechanism and predicting the synthetic waveforms. We emphasize that obtaining reliable focal mechanism solutions requires detailed information about the velocity structures. Unless the velocity structure is adequately known, the simultaneous waveform match on all three components (vertical, radial, and tangential) is almost impossible.

We have also determined a velocity model, Table 2, for the source area by appropriately modifying the original model suggested by Cranswick. However, our

model should not be treated as exact, since the model could not produce enough reverberations in the synthetic seismograms to duplicate those observed. Nonetheless, it is a good starting model for the source region.

The error contained in the focal mechanisms of these earthquakes is difficult to quantify in an absolute sense because of the interdependence of the structure, source-time function, and focal mechanisms on the final waveforms. In addition, the ground motion is a nonlinear function of the depth. In earlier attempt (Saikia and Herrmann, 1984), the focal mechanisms of aftershocks of 1, 3, and 4 were determined, in general, as dip = 25° ± 10°, slip = 120° ± 15°, and strike = 30° ± 15°, using a simple velocity model (P velocity: 6.15 km/sec; S velocity: 3.58 km/sec). This half-space model could produce the wave shapes, but failed to predict the correct amplitude ratios at various components. Even addition of one layer over the half-space could not solve the problem of the amplitude ratios. The amplitude ratios were found to vary a lot with the variation of depth. The waveforms were also sensitive to the focal mechanisms. However, using our suggested model, we were able to predict the amplitude ratios quite successfully. Therefore, the aftershocks of this study must be well constrained both in focal mechanism and depth. Based on this work, we also conclude that the focal mechanisms obtained by simply matching $(SV/P)_z$ amplitude ratios using a simple velocity model and allowing possible trade-off errors in the amplitude ratios may be, sometimes, erroneous.

In our attempt to model the filtered seismograms of these aftershocks in the manner described, much time was spent on producing the appropriate Green's functions. This effort is a worthwhile and necessary first step if we wish to model the observed recordings in detail to study site effects. Such a study will require even more computational effort. If the velocity model is detailed and well established, this method can be implemented on a routine basis, since searching through the parameter space and comparing the waveforms can be performed quickly. Thus, we do not believe that the technique used represents a computational overkill in studying earthquakes recorded at short distances. In fact, it is the only way to obtain consistent focal mechanisms if there are a limited number of observations.

The focal mechanism studies of the aftershocks indicate that the faulting process in the source region of the Miramichi earthquake of 9 January 1982 is associated with an approximately east-west-oriented compressive stress field and is characterized mostly by reverse faulting. The orientations of the fault planes are scattered in true sence. The assumption of a short duration pulse is supported since we modeled low-pass-filtered versions of the observed data rather than the high-frequency data directly.

As pointed out by an unknown reviewer, the difference in amplitude between the phases at some stations is, somewhat, bothersome and cannot be accounted by a single reason. The problem is primarily noticed in the spectral analysis, the seismic moment estimates being different for both P and S waves from the same station. Presumably, modeling with an increased number of generalized rays with differential velocity models incorporating the site effect may reduce this scatter, a study which must, of course, be performed. In the present study, this problem was encountered with the events of 17 January, particularly with the radial component and as pointed out in the text, the cause could be the site conditions. However, time-domain seismic moments show less scatter from station to station than do the spectral seismic moments. This is because in the spectral analysis, we look at many P or S arrivals at a time.

The seismic moments estimated from the spectral analysis are sometimes higher than the values obtained by the time-domain waveform modeling. The *P*-wave corner frequencies are always greater than the *S*-wave corner frequencies. The associated stress drops are very large since the source dimensions are very small.

Finally, we have constructed a model which matched the observed data. We have not really defined the temporal aspects of the source since the source effects are still convolved with other propagation effects, such as site effects and fine velocity structure. This study was valuable in showing that short distance recordings of earthquakes can be modeled, but only if the velocity structure is reasonably well known.

ACKNOWLEDGMENTS

The authors will like to acknowledge Otto W. Nuttli for his many comments during this study and thank E. Cranswick of the U.S. Geological Survey for suggesting the initial velocity model and Tzay C. Shin, Saint Louis University for providing information about the *Q* value of the New Brunswick area. This research was supported by the U.S. Department of the Interior, Geological Survey, under Contracts 14-08-0001-20640 and 14-08-0001-21886, and also by the National Science Foundation under Grant CEE-8406577.

REFERENCES

Aki, K. and P. G. Richards (1980). *Quantitative Seismology Theory and Methods*, vol. I, W. H. Freeman and Company, San Francisco, California, p. 558.

Archuleta, R. J. and S. H. Hartzell (1981). Effects of fault finiteness on near source ground motion, *Bull. Seism. Soc. Am.* **71,** 939–957.

Boatwright, J. (1972). Detailed spectral analysis of two small New York state earthquakes, *Bull. Seism. Soc. Am.* **68,** 1117–1131.

Brune, J. N. (1970). Tectonic stress and the spectra of seismic shear waves from earthquakes, *J. Geophys. Res.* **75,** 4997–5009.

Brune, J. N. (1971). Tectonic stress and the spectra of seismic shear waves from earthquakes: correction, *J. Geophys. Res.* **76,** 5002.

Burdick, L. J., T. Wallace, and T. Lay (1984). Modeling near-field and teleseismic observations from the Amchitka test site, *J. Geophys. Res.* **89,** 4373–4388.

Choy, G. L., J. Boatwright, J. W. Dewey, and S. A. Sipkin (1983). A teleseismic analysis of the New Brunswick Earthquake of January 9, 1982, *J. Geophys. Res.* **88,** 2199–2212.

Cranswick, E., C. Mueller, R. Wetmiller, and E. Sembera (1982). Local multi-station digital recordings of aftershocks of the January 9, 1982 New Brunswick earthquake, *U.S. Geol. Surv., Open-File Rept. 82–777.*

Heaton, T. H. (1978). Generalized ray models of strong ground motion, *Ph.D. Thesis*, California Institute of Technology, Pasadena, California, p. 292.

Helmberger, D. V. and D. G. Harkrider (1978). Modeling earthquakes with Generalized Ray Theory, in *Modern Problems in Elastic Wave Propagation*, J. Miklowitz and J. Achenbach, Editors, John Wiley and Sons, New York, 499–518.

Kisslinger, C. (1980). Evaluation of *S* to *P* amplitude ratios for determining focal mechanisms from regional network observations, *Bull. Seism. Soc. Am.* **70,** 999–1014.

Langston, C. A. (1981). Source inversion of seismic waveforms: The Koyna, India, earthquakes of September 13, 1967, *Bull. Seism. Soc. Am.* **71,** 1–24.

Lawson, C. L. and R. J. Hanson (1974). *Solving Least Squares Problems*, Prentice-Hall, Inc., Englewood Cliffs, New Jersey, 340 pp.

Mendiguren, J. A. (1977). Inversion of surface wave data in source mechanism studies, *J. Geophys. Res.* **82,** 889–894.

Saikia, C. K. and R. B. Herrmann (1984). Modeling of direct *P*- and *S*-phases of 3-local earthquakes of New Brunswick area, Canada (abstract), *EOS* **65,** 240.

Savage, J. C. (1972). Relation of corner frequency to fault dimensions, *J. Geophys. Res.* **77,** 3788–3795.

Snoke, J. A., J. W. Munsey, A. G. Teague, and G. A. Bollinger (1984). A program for focal mechanism determination by combined use of polarity and *SV-P* amplitude ratio data (abstract), Presented at the 56th Annual Meeting of ESSA.

Wetmiller, R. J. J. Adams, F. M. Anglin, H. S. Hasegawa, and A. E. Stevens (1984). Aftershock sequences of the 1982 Miramichi, New Brunswick, earthquake, *Bull. Seism. Soc. Am.* **74**, 621–654.

Wiggins, R. A. (1972). The generalized linear inverse problem: implication of surface waves and free oscillations for earth structure, *Rev. Geophys. Space Phys.* **10**, 251–285.

DEPARTMENT OF EARTH AND ATMOSPHERIC SCIENCES
SAINT LOUIS UNIVERSITY
P.O. BOX 8099, LACLEDE STATION
ST. LOUIS, MISSOURI 63156

Manuscript received 4 February 1985